X-ray emission cross sections for carbon bombarded with 4- to 40-MeV C, N, and O ions*

F. W. Martin

Department of Physics and Astronomy, University of Maryland, College Park, Maryland 20742

W. Freeman and J. Sauls

Department of Physics, State University of New York at Stony Brook, Stony Brook, New York 11974
(Received 28 March 1977)

Cross sections for production of target-atom carbon K x rays in thin evaporated carbon films are determined from spectra obtained using a double-focusing soft-x-ray spectrometer with calibrated transmission. A maximum value of 2.3×10^{-19} cm^2 is found for 18-MeV oxygen ions. A maximum ionization cross section of 4.8×10^{-17} cm^2 is estimated from the data. Cross sections for x rays on both sides of the carbon K edge are determined. Nitrogen ions produce more L-shell ionization at low energies than carbon or oxygen ions, both of which create very few KL^2 satellite x rays below about 9 MeV.

INTRODUCTION

Cross sections for K x-ray production in atomic collisions involving high-velocity ions have been extensively measured, both at velocities below that for a maximum in the cross section[1] and for projectiles of low atomic number.[2] Relatively few measurements are available on K x-ray production at velocities near the maximum in cases where the atomic number Z_1 of the projectile is equal to or greater than the atomic number Z_2 of the target.[3-5] These velocities can be attained with available accelerators if Z_2 is small, since the projectile velocity V can then be made larger than the velocity v_K of the electrons in the target K shell. However, when Z_2 is small the x rays emitted occur in the soft-x-ray region, in which both Si(Li) semiconductor detectors and proportional counters have poor resolution.

The present experiment uses a high-resolution soft-x-ray spectrometer to determine x-ray cross sections for projectiles with $Z_1 \simeq Z_2 = 6$ with $V \simeq v_K$. A comparison to available theories for the K-shell ionization is made by estimating the fluorescence yield for various portions of the observed soft x-ray spectral distribution. The biologically important carbon atom was chosen as a target because of the need for basic data to assess the usefulness of x-ray emission in high-resolution scanning ion microscopy.[6,7]

EXPERIMENT

For these measurements a double-focusing soft x-ray spectrometer especially made for ion-atom collision studies[8] was installed at a tandem Van de Graaff laboratory, and procedures developed in experiments below 3 MeV[9] were applied to obtaining absolute cross sections. Therefore the configuration of the apparatus will be summarized,

and only differences and extensions from previous work will be described in detail. The spectra on which these measurements are based are the subject of a separate article.[10]

Before reaching the target, ions from the accelerator passed through a 90° energy-analyzing magnet, a triplet of quadrupole focusing magnets, a removable carbon prefoil of 5 μg/cm^2 thickness, a 15° beam-switching magnet, and a collimating system consisting of (1) a fixed circular aperture of $\frac{3}{8}$ in. diameter followed by (2) a square aperture HV of 0.060 in. dimension, the position of which was adjustable in two dimensions perpendicular to the beam direction, and (3) an anti-scattering collimator AS of $\frac{1}{8}$ in. diameter aligned optically on line with the center of the spectrometer. The counting rate of the spectrometer was found to have a broad maximum as the HV slits were traversed in the plane of the Rowland circle, and the HV slits were adjusted vertically and horizontally in line with the AS collimator, using measurements of transmitted beam current. The dimensions of the system were such that the maximum beam width or height at the target was $s = 0.138$ in, while collimator AS prevented any ions scattered from the slits of aperture HV from striking the target-holding frame. Targets were mounted on a foil wheel, the axis of which made an angle θ_T with respect to the beam direction. The observation angle θ_E between the emerging x-ray direction and the beam is independently adjustable in the spectrometer and was set so that the grazing angle $\theta_G = \theta_T - \theta_E + \frac{1}{2}\pi$ between the foil surface and the observation direction was small. Ideally θ_G should be zero, so that the width $d = s \sin\theta_G \sec\theta_T$ of the foil which emits x rays, as viewed from the observation direction, is much smaller than the acceptance width A of the spectrometer; however, θ_G cannot be exactly zero because of the target holder, nor can it be too small because of exces-

TABLE I. Calibration data. Calculations made using Eqs. (4), (33), and (18) of Ref. 8, and as described in text. Detector slit width $W = 0.063$ in., foil thickness 50 $\mu g/cm^2$, target inclination angle $\theta_T = 145°$, grazing angle $\theta_G = 29°$.

Bragg angle θ (deg)	27.2	61.0	27.2	61.0
Projected maximum spot width d (mils)	82	82	82	82
Spectrometer acceptance A (mils)	60	115	60	115
Spectrometer geometrical resolution w (mils)	55	31	55	31
Spectrometer constant K	3.2×10^6	6.3×10^6	2.1×10^6	3.6×10^6
Solid angle Ω_x (sr)	2.1×10^{-2}	7.5×10^{-2}	2.1×10^{-2}	7.5×10^{-2}
Efficiency ϵ_x	1.8×10^{-5}	0.51×10^{-5}	2.8×10^{-5}	0.91×10^{-5}
Number of measurements	1	3	2	3
rms deviation of values	...	1%	17%	3%

sive self-absorption in the foil.

Values of d and A are shown in Table I. The spectrometer acceptance A was estimated from the angular width over which the pseudocrystal will diffract x rays of a constant wavelength; the geometrical contribution w was smaller than A. The targets were commercial[11] amorphous carbon films of 5 or 50 $\mu g/cm^2$ thickness with a thickness uncertainty of 5%. Particles scattered at an angle θ_R with respect to the beam were detected with a semiconductor particle detector subtending a solid angle of 1.26×10^{-4} sr. Beam current ranged from 0.3 to 100 nA, depending on charge state, multiple scattering in the prefoil, and focusing.

Calibration of the spectrometer with a new channeltron detector and a new 2000-Å silver foil installed was carried out using the procedure previously described, except that 4 MeV protons scattered at $\theta_R = 20°$ were used. At this small angle proton scattering still follows the Rutherford formula even at 9.5 MeV.[12] Normalization was to an x-ray emission cross section of 1.09×10^{-21} cm^2 for 4.0 MeV protons calculated from a measured Auger cross section of 0.75 ± 0.10 cm^2 for 2 MeV protons,[13] a measured fluorescence yield $\omega = 2.2 \times 10^{-3}$,[14] and a measured decrease in the relative proton-induced x-ray cross section from 2 to 4 MeV.[15] This value agrees with direct measurements at 4 MeV.[16] The spectrometer was calibrated twice, with values shown in Table I. The angle of the semiconductor detector at which $\theta_R = 0$ was carefully determined within 0.1° for one calibration by measuring elastic scattering on each side of the beam. Data were reduced using one calibration up to a certain time and another afterwards. The 40% deviation between calibrations at the same Bragg angle but different times, which is possibly associated with misalignment of the semiconductor detector in the period between calibrations, serves as an indication of the systematic error to be expected in the data. In addition, 17 early measure-

ments on first-order oxygen-induced spectra, for which no calibration was available because of a broken silver foil, were normalized into later data. This normalization affects only results shown in Fig. 1.

Self-absorption of x rays in the target affected any measurements which were not taken with the same grazing angles θ_G as the calibrations. The fraction R of x rays generated within a target which escape is given by

$$R(\theta_G, \lambda) = (1 - e^{-T})/T \qquad (1)$$

where $T = t\rho\mu \csc\theta_G$, $t\rho$ is the target thickness in $\mu g/cm^2$, and $\mu(\lambda)$ is the absorption coefficient in cm$^2/\mu g$. Values $\mu_L = 2.23$ cm^2/mg and $\mu_U = 53.9$
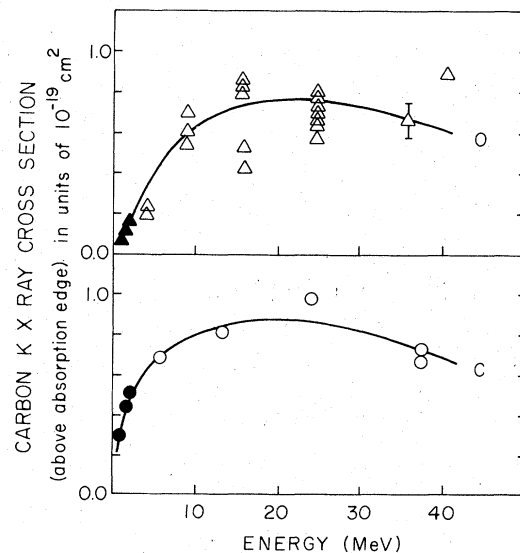

FIG. 1. Cross sections σ_L for K x-ray emission from evaporated carbon foil at x-ray wavelengths above the carbon absorption edge as a function of the energy of the exciting ion. Top section: O ions. Bottom section: C ions. Filled symbols: Data of Ref. 9.

cm^2/mg were taken from tabulated extrapolated jump ratios.[17]

A further factor in treatment of the data is the reduced transmission of the spectrometer for x rays with energies above the absorption edge of the pseudocrystal. From values of the integrated reflection efficiency of 5.0×10^{-5} and 3.8×10^{-4} on either side of the edge,[18] it was estimated that the spectrometer efficiency ϵ_x decreased by a factor of 7.6 for these x rays.

In the analysis of spectra, a computer fit of a linear background was made to the data above and below the spectral peaks, and the area X_{TL} above background under the main peak and at Bragg angles larger than θ_A was computed. Similarly, the area X_{TU} above background under the satellite peak and at Bragg angles smaller than θ_A was computed. Sufficient statistics were accumulated to enable this procedure, which was done with an on-line display of peaks and computed background. The value of θ_A was selected using a light pen in the region $60° < \theta_A < 61°$, corresponding to $281 < E_A < 284$ eV. Lacking experimental measurement with a continuum x-ray source, it is difficult to state exactly where the absorption edge is located. However the binding energy of 283.6 eV for $1s$ electrons in graphite is quite close to the value of 284.1 for ethanol and 284.3 for cyclohexane determined by electron-spectroscopy-for-chemical-analysis (ESCA) methods for the condensed solid form of these materials.[19] Shifts of this magnitude, which are characteristic of organic compounds containing only C and H, are much smaller than would be determined using the ESCA values for gases, which differ by the work function of about 5 eV that occurs when the material condenses.[19] Thus, unlike previous authors,[14] we do not expect the KL^2 satellite to be transmitted readily by either the emitter or the carbon-containing x-ray optical system.

In general, the spectra did not exhibit Doppler-shifted lines from the projectiles. A bright line near 300 eV which had the proper dependence on the velocity of the projectile was observed for oxygen ions traversing 5-μg/cm^2 foils, but was decreased approximately tenfold when a 50-μg/cm^2 foil was used. Less intense, broadened, shifting lines were also found near 280 eV in the same case, and accordingly data for 5-μg/cm^2 foils excited by oxygen are excluded from the present report. No shifting lines were noted for carbon or nitrogen ions and 50-μg/cm^2 foils. In the case of carbon ions, the projectile radiation is expected to be strongly quenched since the radiative lifetime is much larger than the time for the projectile to enter another vacancy-producing collision.[20] It may be concluded that even for carbon ions the measurements pertain to target K x-ray cross sections.

Cross sections were computed using

$$\sigma = K\sigma_R X_T / R \qquad (2)$$

where R is the number of scattered particles per step, X_T is the total number of counts in a peak, σ_R is the Rutherford cross section for projectile scattering and target recoil into the detector,[9] and $K = 4\pi(\Delta\theta)/\tau\epsilon_x\Omega_x$ is the spectrometer calibration constant[8] for a given order and standard values $\theta_{GC} = 29°$, $t_C\rho = 50$ μg/cm^2. Cross sections computed from values of X_{TL} obtained at nonstandard θ_G and $t\rho$ were corrected using Eq. (1) to give values σ_L, while those computed from values of X_{TU} were corrected similarly and further multiplied by the factor of 7.6 to give values σ_U. The cross section σ_x for production of K x rays was taken as the sum of these values. Estimated errors in this procedure and their sources are listed in Table II, and example random errors are entered on the figures. The results shown in a single section of Fig. 2 involve measurements made on a single day, so that the scatter of data in this figure should reflect only the random error.

In some cases it has been found that the x-ray production cross section is a function of the charge of the projectile as it enters the x-ray producing collision.[21-23] In the present case this effect should be small because of the extremely short distance required for the projectile to come to charge-state equilibrium in the solid. From measurements of the electron capture and loss cross sections for oxygen ions colliding with nitrogen,[24] the target thickness for e^{-1} of the incident ions to capture or lose one or more electrons may be estimated as 0.2 μg/cm^2 for 9-MeV O^{+3} ions and 3.2 μg/cm^2 for 36-MeV O^{+6} ions. Since these distances are smaller than the foil thickness as well as the character-

TABLE II. Estimated errors.

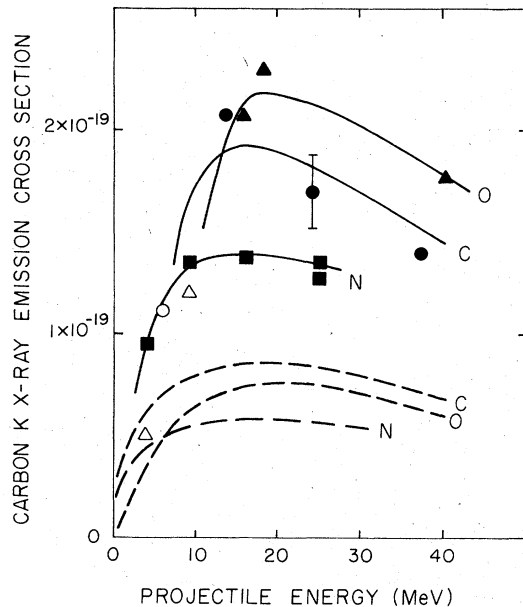| Source	Percentage error in	
	σ_U	σ_L
Random errors:		
Background relative to peak height	10	0.5
Statistical error, $(X_T)^{-1/2}$	5	0.5
$\Delta\theta_G = \pm 3°$	10	2
Probable random error from above 3 sources	15	2
Systematic errors:		
$\Delta t/t = 5\%$	5	5
$\Delta\mu/\mu = 4\%$	4	4
Reflection efficiency	15	...
$\Delta\theta_R = \pm 1°$	20	20
Calibration constant	20	20
Probable systematic error from above 5 sources	32	28

FIG. 2. Experimental points: Cross sections $\sigma_x = \sigma_L + \sigma_U$ for carbon K x-ray emission on both sides of the carbon absorption edge as a function of the energy of the exciting ion for C ions (circles), N ions (squares) and O ions (triangles). The open symbols represent upper limits. Solid lines: Curves drawn through the experimental data for each ion. Dashed lines: Curves for σ_L from Fig. 1. Doppler-shifted radiations from the projectile were not observed in the wavelength regions of interest in the spectra which were integrated to obtain these cross sections.

istic distance $(\mu_U)^{-1} \sec\theta_T \sin\theta_G = 11$ $\mu g/cm^2$ in which high-energy x rays are absorbed, it may be concluded that most ions entering collisions which are observed to produce x rays will be in an equilibrium charge distribution. K-shell vacancy equilibrium occurs at target thicknesses less than $(\sigma_v)^{-1}$, corresponding to less than 2.5 $\mu g/cm^2$,[20] and should therefore not be an important parameter. The experimental measurements should thus be characteristic of ions with the equilibrium charge and equilibrium excitation rather than the incident charge and incident excitation.

These considerations were experimentally checked by using the prefoil and switching magnet to direct ions of different charge states onto a 5-$\mu g/cm^2$ foil. For 25-MeV O^{+n} ions, there was no charge dependence larger than the random error for $5 \leq n \leq 8$. For 16-MeV N^{+n} ions there was inconclusive evidence that +4 ions produce more x rays than +5 or +6 ions, perhaps because the +4 ions, prepared at 3 MeV in the accelerator terminal, have a different K-vacancy fraction than the higher charge ions, prepared at 16 MeV in the prefoil.

RESULTS

Cross sections σ_L for emission of carbon K x rays with wavelengths above the absorption edge of the pseudocrystal are shown in Fig. 1. The curves are drawn by hand. Points below 3 MeV are taken from earlier work.[9] Cross sections σ_x for emission of x rays on both sides of the absorption edge

TABLE III. Carbon K x-ray production cross sections for high-energy ions colliding with evaporated carbon foils.

Ion	Incident charge	Energy (MeV)	σ_L $(10^{-20} cm^2)$	σ_U $(10^{-20} cm^2)$	σ_x $(10^{-20} cm^2)$	$t\rho$ $(\mu g/cm^2)$	θ_G (deg)	θ_T (deg)	θ_R (deg)
C	+5	37.5	7.2	6.8	14.0	5	29	145	10
	+5	37.5	6.6			50	29	145	10
	+4	24.0	9.7	7.2	16.9	50	29	145	20
	+3	13.5	8.0	12.7	20.7	50	29	145	20
	+2	6.0	6.9	<4	<11	50	29	145	18.3
N	+4	25.0	5.5[a]	7.1[a]	12.6[a]	50	80[a]	145	20
	+4	25.0	5.4	8.1	13.5	50	29	145	20
	+4	16.0	4.6[a]	9.0[a]	13.6[a]	50	80[a]	145	20
	+3	9.0	5.1	8.4	13.5	50	29	145	20
	+3	9.0	5.1			5	29	145	20
	+2	4.0	1.74			50	29	145	20
	+2	4.0	2.6	6.8	9.4	50	29	145	20
O	+6	40.5	8.8	9.1	17.9	50	29	145	10
	+4	18.0	9.2	13.9	23.1	50	29	145	10
	+4	16.0	8.0	12.8	20.8	50	20	145	20
	+3	9.0	5.6	<6	<12	50	19	154	20
	+2	4.0	2.1	<3	<5	50	19	154	30

[a]Incomplete collection at $\theta_G = 80°$, values about 30% low.

are tabulated with relevant experimental param-
eters in Table III and are plotted in Fig. 2. In this
figure the dashed lines duplicate the curves drawn
through the data of Fig. 1, and the solid lines are
drawn by hand.

DISCUSSION

A. K-shell ionization cross sections

In order to compare experimental x-ray pro-
duction cross sections to theoretical ionization
cross sections, a value of the fluorescence yield
ω is required. For collisions involving heavy ions,
which produce multiple atomic ionizations, the
fluorescence yield may rise considerably above the
value for atoms with single K vacancies. An in-
dication of this effect is the presence of satellite
lines in the x-ray emission spectrum. The spec-
tra of the present experiment have been interpre-
ted as exhibiting KL and KL^2 satellites,[10] and flu-
orescence yields for each satellite are available.[25]
Ionization cross sections σ_I estimated from the da-
ta by assuming that σ_L contains contributions only
from K and KL lines with an average $\omega_L = 2.5$
$\times 10^{-4}$, while σ_U contains only KL^2 lines with ω_U
$= 13.0 \times 10^{-4}$, are shown in Fig. 3.[26] It is apparent
that σ_U does not contribute strongly to the ioniza-
tion cross section, because of the large value of
ω_U, and that consequently uncertainties in ϵ_x, θ_A,
and ω_U do not have a large effect on the estimated
value of σ_I.

It is very difficult to construct a theory of K-shell
vacancy production which is valid over a region of
velocity spanning the maximum in the cross sec-
tion. For $V < v_K$ the molecular-orbital model of
$2p\sigma$-$2p\pi$ electron promotion by rotational coupling
in the united atom has been successfully used, and
scaling procedures devised for both symmetric[27]
and asymmetric[28] collisions. However these papers
rule out consideration of the translation factors[29,30]
which are necessary at high velocities. Even when
translation factors are used[31] in a molecular-or-
bital theory of rotational coupling, the momentum
factor only is brought in and the energy factor
$\exp(imV^2t/2\hbar)$ is ignored. This factor changes the
phase of the state functions and, since it separa-
tes the energies of the states by $\frac{1}{2}mV^2$, it makes
the internuclear separation at which level cross-
ing occurs depend on projectile velocity.[32]

An alternative theory for K-shell ionization, not
including electron capture by the projectile, is pro-
vided by the plane-wave Born approximation,
(PWBA) including corrections for projectile de-
flection and for alteration of binding energies dur-
ing the collision.[33] This theory gives good agree-
ment with experiment when $Z_1 < Z_2$, and it may be
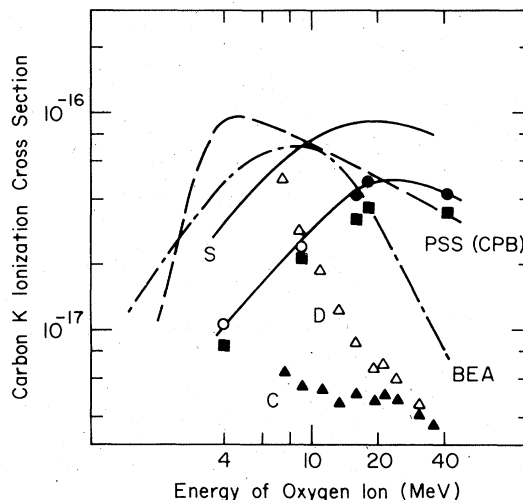modified to account for distortion of the atomic

FIG. 3. Ionization cross sections estimated from the
x-ray cross sections for oxygen ions. Squares: Partial
cross sections estimated from values of σ_L using an
average of theoretical fluorescence yields for K and KL
satellite emission. Circles: Total cross sections ob-
tained by adding a contribution from σ_U estimated using
a theoretical fluorescence yield for the KL^2 satellite.
Open circles: Upper limits to the total cross section.
A solid curve is drawn by hand through the circles.
Dashed curve: PWBA theory with corrections for in-
creased binding, Coulomb deflection, and polarization.
Dot-dashed curve: Binary encounter approximation.
Both theories do not apply when $Z_1 \simeq Z_2$ and are included
only for reference. Curve labeled S: PWBA without
correction for polarization, multiplied by a factor $(Z_{av}/Z_1)^2$. Points labeled C: Approximate magnitude of elec-
tron capture by projectile from target K shell. Points
labeled D: Approximate capture from K and L shells.

wave functions during the collision by projectiles
of higher Z_1.[34] Similar theories have been for-
mulated for electron capture.[35]

In Fig. 3 the PWBA as modified for deflection,
binding energy, and distortion[36] is compared with
ionization cross sections estimated from the data
for oxygen projectiles. This theory is only valid
for $Z_1 < Z_2$, and should not be expected to agree
with the data. The binary-encounter approxima-
tion[37] is also plotted in the figure for reference.
At high energies the agreement in magnitude be-
tween the PWBA and the data is satisfactory, if
the systematic error in the measurements and the
arbitrary assumption of an average fluorescence
yield for K and KL lines are considered. However
the logarithmic plot shows clearly that the data
do not have the energy dependence predicted by
the theories, both of which predict too steep a
rise below the maximum and a maximum at too low
a velocity.

The disagreement is probably associated with
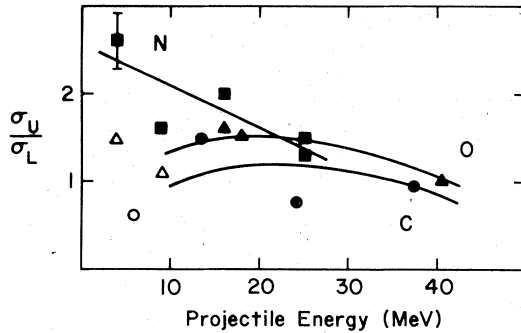screening of the projectile charge. The adiabatic

FIG. 4. Ratio σ_U/σ_L as a function of energy. The curves are drawn through the data for C ions (circles), N ions (squares) and O ions (triangles) and the open symbols represent upper limits. This ratio gives a measure of the excitation of the KL^2 satellite relative to the K and KL lines. Nitrogen ions produce anomalously large L-shell ionization at low energies.

impact parameter $\hbar V/E_K$, where E_K is the binding energy of the carbon K shell, lies between $0.3a_0$ and a_0 for projectile velocities of the experiment, so that the projectile can ionize atoms in collisions with impact parameters greater than its own K-shell radius, or even its own ionic L-shell radius. In Fig. 3 the curve labeled S is the PWBA without distortion,[33] corrected by the ratio $(Z_{av}/8)^2$, where Z_{av} is the average charge observed outside carbon foils.[38] The maximum at 18 MeV is predicted, but the magnitude is a factor of 2 larger than observed. Presumably, the combined effects of the PWBA

with polarization and projectile screening are required, as is the case for oxygen in aluminum.[39]

Figure 5 shows the present measurements together with ionization cross sections for various ions over a large range of velocity. Ionization cross sections σ_I divided by Z_1^2 are plotted as a function of the energy per unit mass of the projectile. It is apparent that R, which is the ratio of σ_I/Z_1^2 for a heavy ion to σ_I for a proton at the same velocity, is less than unity over a considerable range of velocities for all three ions, and that the reduction in R causes the maximum in the cross section to occur at a higher velocity than for protons.

The relative importance of ionization to the continuum and ionization by electron capture may be estimated using experimental data for the similar target atom nitrogen. In Fig. 3 are shown approximate average K-shell electron capture cross sections

$$(\sigma_{87} + \sigma_{86})\phi_8 + \sigma_{76}\phi_6$$

as a series of points C and approximate total electron capture cross sections

$$\sum_{i=0}^{z_1} (\sigma_{i,i-1} + \sigma_{i,i-2})\phi_i$$

as a series of points D. These estimates are computed using experimental cross sections $\sigma_{ij}(V)$ for capture of one or two electrons by oxygen ions of charge i from nitrogen molecules[24] and equilibrium fractions $\phi_i(V)$ for oxygen outside carbon.[38] The
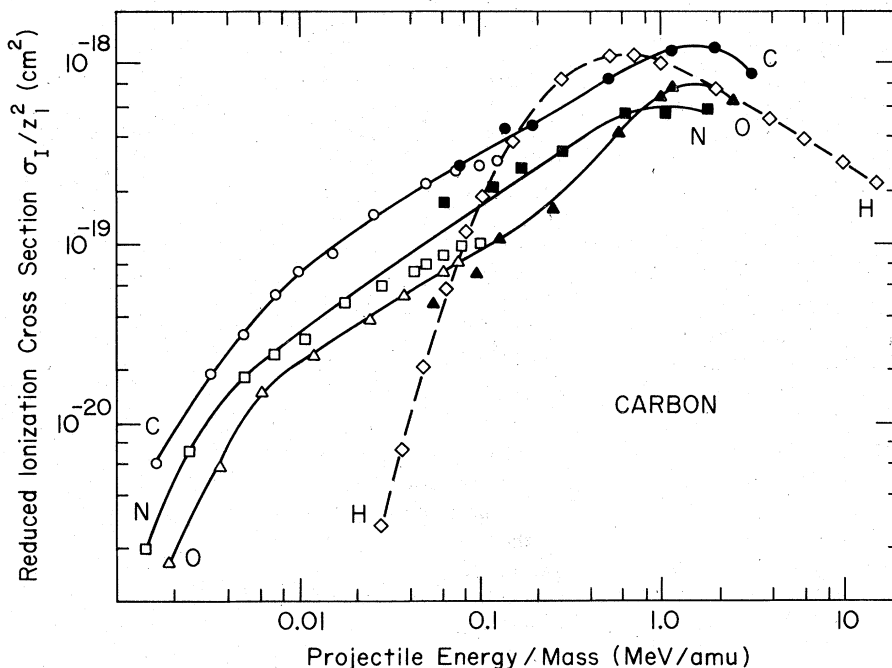

FIG. 5. Carbon K ionization cross sections σ_I, divided by Z_1^2. The curves are drawn by hand through the filled symbols, representing the present measurements and those of Ref. 9 for C, N, and O ions. The open symbols are computed from MeV target values of ionization cross sections as stated in Refs. 46 and 47. The cross section for carbon is not divided by 2. The dashed curve and diamonds are experimental data for protons from Refs. 16 and 48.

trend of these data suggests that electron capture is not an important process in producing K vacancies, at least at the higher velocities of this experiment.

B. L-shell ionization

The partial cross section σ_U provides a measure of L-shell ionization, since it involves only the KL^2 satellite. The data of Table III show that there seems to be a threshold value for this cross section at about 9 MeV for C and O ions. By contrast the binary-encounter-approximation (BEA) model and other ionization theories applied to the L shell predict decreasing ionization at all velocities measured, because $V/v_L \gg 1$. It is noteworthy that the probability of electron capture from the loosely bound helium atom by $+8$ oxygen ions reaches a maximum of about 0.1 at 20 MeV,[40] and it is therefore possible that the threshold in σ_U is associated with the appearance of $+8$ ions in the oxygen beam as it traverses the solid target foil. Below 10 MeV, $+8$ ions are less than 1% abundant in carbon foil.[38]

Figure 4 shows that ratio σ_U/σ_L is anomalous at low energies for nitrogen ions. This coincides with the previous observation of the KL^2 line only for nitrogen at energies below 3 MeV. In this work it

was argued that a $3d\pi \to 3d\sigma$ "demotion" process in the united atom was responsible for the KL^2 emission. Why should such a process not also produce the KL^2 line when oxygen is the projectile? A possible answer is that an appreciable flux of O^{+6} ions incident upon C atoms is required to produce a visible KL^2 satellite.[41] The ions required for this process are not available at low energies, since the equilibrium population of O^{+6} ions in carbon only reaches 50% at 10 MeV. In contrast, the equilibrium population of the corresponding N^{+5} ions in carbon reaches 50% at about 5 MeV.[38]

The generation of KL^2 satellites may thus be associated with electron transfer from the target L shell into the projectile K shell (best described by an atomic orbital theory) for $V > u_K$, and with transfer of initial L-shell vacancies on the projectile into the target L shell (best described by a molecular orbital theory) for $V < u_K$.

*Work supported by ERDA Contract No. AT(11-1)-2454 and by the National Science Foundation.
[1]J. D. Garcia, R. J. Fortner, and T. M. Kavanagh, Rev. Mod. Phys. 45, 111 (1973).
[2]C. H. Rutledge and R. L. Watson, At. Nucl. Data Tables 12, 195 (1973).
[3]J. R. Mowat, I. A. Sellin, P. M. Griffin, D. J. Pegg, and R. S. Peterson, Phys. Rev. A 9, 645 (1974).
[4]F. Hopkins, R. Brenn, A. R. Whittemore, N. Cue, and R. P. Chaturvedi, Phys. Lett. 53A, 79 (1975).
[5]L. Winters, M. D. Brown, L. D. Ellsworth, T. Chiao, E. W. Pettus, and J. R. Macdonald, Phys. Rev. A 11, 174 (1975).
[6]F. W. Martin, Science 179, 173 (1973).
[7]F. W. Martin, Optik (Stuttg.) 40, 484 (1974).
[8]F. W. Martin and R. K. Cacak, J. Phys. E 9, 662 (1976).
[9]R. K. Cacak and F. W. Martin, Phys. Rev. A 13, 599 (1976).
[10]F. W. Martin, W. Freeman, and J. Sauls, J. Phys. B 10, L439 (1977).
[11]Manufactured by the Arizona Carbon Foil Co., Tucson, Ariz. 85711.
[12]W. E. Burcham, W. M. Gibson, A. Hossain, and J. Rotblat, Phys. Rev. 92, 1266 (1953).
[13]L. H. Toburen, Phys. Rev. A 5, 2482 (1972).
[14]A. Langenberg and J. van Eck, Phys. Rev. Lett. 31, 71 (1973).
[15]D. Burch, Phys. Rev. A 12, 2225 (1975).
[16]G. Bissinger, J. M. Joyce, and H. M. Kugel, Phys.

Rev. A 14, 1375 (1976).
[17]B. L. Henke and E. S. Ebisu, Adv. x-Ray Anal. 17, 151 (1973).
[18]B. L. Henke and M. A. Tester, Adv. x-Ray Anal. 18, 76 (1975).
[19]U. Gelius et al., Phys. Scripta 2, 70 (1970).
[20]When parameters of the present experiment are used in expressions for the K-vacancy equilibrium fraction (Ref. 42), the equilibrium distance is found to be shorter than the foil thickness and the dynamic fluorescence yield is found to be small. The unperturbed lifetime τ of a K vacancy in a carbon projectile is approximately the Auger emission time $\tau_R = 1.0 \times 10^{-14}$ sec (Ref. 43) and the effective cross section $(nv\tau)^{-1}$ is smaller than the value of about 2×10^{-19} cm^2 for the lowest-energy ions. The smallest target vacancy-production cross section determined herein is 1×10^{-17} cm^2. Since the molecular orbital (MO) model predicts vacancy sharing for symmetric collisions and high velocities (Ref. 31), this may be taken as the smallest projectile vacancy-production cross section σ_v. Capture cross sections σ_c into the K shell are unknown but $\sigma_c + \sigma_v > \sigma_v = 1 \times 10^{-17}$ cm$^2 > 2 \times 10^{-19}$ cm$^2 > \sigma$ and $\sigma_T = \sigma_v + \sigma_c + \sigma > \sigma_v > (x_0)^{-1}$ where $x_0 = 20 \times 10^{17}$ atoms/cm^2 is the target thickness for the thicker foils. When these two inequalities are fulfilled (Ref. 42), the dynamic fluorescence yield $\omega' = (\sigma/\sigma_T)\omega$ is more than a factor of 50 smaller than ω.
[21]T. J. Gray, P. Richard, K. A. Jamison, J. M. Hall, and R. K. Gardner, Phys. Rev. A 14, 1333 (1976).

The procedure of calculation consists of adding terms of the form

$$x_i/\omega_i = (1-\beta_i)s_i' = -\beta_i s_i' + s_i + \beta_{i+1}s_{i+1}'$$

and when this is done the primed terms cancel, leaving

$$\sum_i x_i/\omega_i = \sum_i s_i \ .$$

Writing out the cascade terms involved in s_0' shows clearly that the diagram line, which would have the intensity $x_0 = \omega_0 s_0$ in a gas, in fact has the larger intensity $x_0 = \omega_0 s_0'$.

[22]F. W. Martin and R. K. Cacak, Phys. Rev. A 13, 643 (1976).

[23]W. Brandt, R. Laubert, M. Morino, and A. Schwarzchild, Phys. Rev. Lett. 30, 359 (1973).

[24]J. R. Macdonald and F. W. Martin, Phys. Rev. A 4, 1965 (1971).

[25]L. H. Toburen, Phys. Rev. A 6, 2035 (1972).

[26]Reference 10 states that it is not possible to determine from the data whether the weak satellites are caused by weak production of vacancies or by strong production of vacancies followed by quenching from the electron gas of the solid. Reference 49 states that "the mean fluorescence yield could be different" because of "capture" of L electrons, and Ref. 10 explicitly discusses the alteration of fluorescence yield by quenching. However, the procedure stated in the text gives the correct cross section even if the spectra result from extensive quenching, so long as fluorescence yields for the isolated atom are used in the calculation. If the branching ratios for x-ray emission, Auger emission, and plasma quenching in a solid are b, γ, and β, respectively, so that $b + \gamma + \beta = 1$ for a given satellite, and if the vacancy-production cross section for the satellite configuration i is s_i while the corresponding partial x-ray cross section is x_i, then for each satellite

$$x_i = b_i s_i' = \omega_i(1-\beta_i)s_i'$$

where the term $s_i' = s_i + \beta_{i+1}s_{i+1}'$ reflects the effect of cascading from higher configurations.

[27]J. S. Briggs and J. H. Macek, J. Phys. B 6, 982 (1973).

[28]K. Taulbjerg, J. S. Briggs, and J. Vaaben, J. Phys. B 9, 1351 (1976).

[29]D. R. Bates and R. McCarroll, Proc. R. Soc. A 245, 175 (1958).

[30]D. R. Bates, Proc. R. Soc. A 247, 294 (1958).

[31]K. Taulberjerg, J. Vaaben, and B. Fastrup, Phys. Rev. A 12, 2325 (1975).

[32]Equation (14) in Ref. 29 contains an energy factor (in atomic units) $\exp(ivZ/2)$, while Eq. (15) contains a momentum factor $\exp(-ivz_1)$.

[33]G. Basbas, W. Brandt, and R. Laubert, Phys. Rev. A 7, 983 (1973).

[34]W. Brandt, in Atomic Physics III, Proceedings of the Third International Conference on Atomic Physics, Boulder, Colo., 1972, edited by S. J. Smith and G. K. Walters (Plenum, New York, 1973), p. 155.

[35]G. Lapicki and W. Losonsky, Phys. Rev. A 15, 896 (1977).

[36]George Basbas (private communication).

[37]J. H. McGuire and P. Richard, Phys. Rev. A 8, 1374 (1973).

[38]A. B. Wittkower and H. D. Betz, At. Data 5, 123 (1973).

[39]R. Laubert and W. Losonsky, Phys. Rev. A 14, 2043 (1976).

[40]F. W. Martin and J. R. Macdonald, Phys. Rev. A 4, 1974 (1971).

[41]That is, assuming that the L-shell electrons are shared among the collision partners, an O^{+6} ion and a C atom will result in ions with an average of $2\frac{1}{2} L$ electrons each, after promotion of a carbon K electron. The carbon will emit a KL^2 line if it receives the 2 electrons and is not quenched before emitting. Thorough sharing of electrons in high-velocity collisions at small impact parameters has been observed experimentally (Refs. 44, 45).

[42]H. D. Betz, F. Bell, H. Panke, G. Kalkoffen, M. Welz, and D. Evers, Phys. Rev. Lett. 33, 807 (1974).

[43]D. Walters and C. Bhalla, Phys. Rev. A 3, 1919 (1971).

[44]F. W. Martin and R. K. Cacak, in Proceedings of the Fourth International Conference on Beam-Foil Spectroscopy and Heavy-Ion Atomic Physics, Gatlinburg, Tenn., 1975 (Plenum, New York, 1976), p. 671.

[45]B. Rosner and D. Gur, Phys. Rev. A 15, 70 (1977).

[46]R. J. Fortner, B. P. Curry, R. C. Der, T. M. Kavanagh, and J. M. Khan, Phys. Rev. 185, 164 (1969).

[47]R. C. Der, R. J. Fortner, T. M. Kavanagh, and J. M. Khan, Phys. Rev. A 4, 556 (1971).

[48]K. G. Harrison, H. Tawara, and F. J. DeHeer, Physica 66, 16 (1973).

[49]R. J. Fortner and D. J. Matthews, Phys. Rev. A 14, 2357 (1976).